Journal of the European Ceramic Society **9** (1992) 83–93

Development and Characterization of Electroconductive Si_3N_4–TiN Composites

A. Bellosi, S. Guicciardi & A. Tampieri

CNR-IRTEC, Research Institute for Ceramics Technology, via Granarolo 64, I-48018 Faenza, Italy

(Received 19 March 1991; revised version received 24 May 1991; accepted 20 June 1991)

Abstract

Dense Si_3N_4–TiN composites, with the second phase ranging from 20 to 40 vol.%, were produced by hot pressing, gas-pressure sintering and pressureless sintering under nitrogen gas atmosphere. The influence of densification technique and parameters and of amount and grain size of TiN particles on microstructure, mechanical properties, electrical resistivity and oxidation resistance was evaluated. The addition of TiN particles increases the stiffness and the fracture toughness of the base material. For TiN content higher than 30 vol.% the electrical resistivity of the composites is less than 10^{-3} Ωcm. An evident effect of the grain size distribution of TiN powders on some mechanical properties was ascertained. The thermal stability of the composites is strongly affected by the amount of the second phase.

Dichte Si_3N_4–TiN Verbundwerkstoffe mit einem Anteil von 20 Vol.% bis 40 Vol.% an TiN wurden mittels Heißpressen, Gasdrucksintern und drucklosem Sintern unter Stickstoffatmosphäre hergestellt. Der Einfluß des Sinterverfahrens, der Versuchsparameter und des TiN-Anteils und der TiN–Korngröße auf das Gefüge, die mechanischen Eigenschaften, die elektrische Leitfähigkeit und die Oxidationsbeständigkeit wurde untersucht. Die Zugabe des TiN erhöht die Steifigkeit und die Bruchzähigkeit des Ausgangsmaterials. Bei einem Anteil, der 30 Vol.% TiN übersteigt, liegt der elektrische Widerstand des Verbundwerkstoffs unter 10^{-3} Ωcm. Ein direkter Einfluß der Korngrößenverteilung des TiN-Pulvers auf einige mechanische Eigenschaften konnte nachgewiesen werden. Die thermische Stabilität der Verbundwerkstoffe hängt stark vom Anteil der zweiten Phase ab.

Des composites Si_3N_4–TiN denses, dont la seconde phase représente 20 à 40% en volume, ont été produits par frittage sous charge, frittage sous pression de gaz et frittage naturel sous atmosphère azote. On a évalué l'influence de la technique et des paramètres de densification, de la quantité et de la granulométrie des particules de TiN, sur la microstructure, les propriétés mécaniques, la résistivité électrique et la résistance à l'oxydation. L'addition de particules de TiN augmente la dureté et la ténacité du matériau de base. Pour une teneur en TiN supérieure à 30% en volume, la résistivité électrique des composites est inférieure à 10^{-3} Ω cm. L'effet de la distribution granulométrique des poudres de TiN sur quelques propriétés mécaniques est mis en évidence. La stabilité thermique des composites est fortement influencée par la quantité de seconde phase.

1 Introduction

The need for improvement in the mechanical reliability of silicon nitride has recently led to the development of high-strength and high-toughness ceramics, such as whisker-reinforced or particulate-reinforced ceramics.[1–5] The degree of toughening is strongly affected by the shape of the dispersoids, whiskers being several times more effective than equiaxed particles; owing to process problems, to reliability problems and to the cost of whiskers, however, increasing attention is being devoted to particulate additions.

This approach has stimulated the development of reinforced ceramics with an electrically conductive second phase,[6–12] which have been considered recently for specific applications in the field of heaters, igniters and heat exchangers and also for

Journal of the European Ceramic Society 0955-2219/92/$5.00

complex-shaped mechanical components. Among the second phases, nitrides (TiN), borides (TiB_2, ZrB_2) and carbides (TiC), whose resistivity is in the range $1{\cdot}4$–$5{\cdot}3 \times 10^{-5}\,\Omega$cm, can be employed. The new type of composite has two main advantages: the first is the possibility of using electrical discharge machining (EDM)[8,13,14] to manufacture complex shapes, the second is the availability of materials suitable for high-temperature heaters and igniters. The electrical conductivity of these materials is directly dependent on the size and amount of the conductive particles. Obviously the second-phase reinforcement should allow retention or improvement of the mechanical properties of the base-line material at room temperature as well as at high temperature.

This study is devoted to Si_3N_4–TiN composites and compares the microstructure development and the properties in relation to the sintering process. Because the development of microstructure is influenced by processing and by the physico-chemical interactions of constituents during sintering and because the properties are strictly related to the grain size of the dispersoids, TiN powders with two different grain size distributions were used. Moreover, electrical discharge machining tests were performed and the treated surfaces were characterized.

2 Experimental Methods

2.1 Materials and methods

Si_3N_4 (LC12, Starck, FRG) and TiN (grade C, Starck, FRG) commercial powders were used. Silicon nitride powders and sintering aids (3 wt% Al_2O_3 (Alcoa A16 S.G., USA) and 8 wt% Y_2O_3 (Rhone-Poulenc, France)) were homogenized in water for 48 h and then freeze-dried. The second phase, ranging from 20 to 40 vol.%, was added to the mix and homogenized in isobutyl alcohol. Green bodies for gas-pressure sintering and for pressureless sintering were produced by cold isostatic pressing and the values of the green densities ($\approx$60%) resulted independently from the presence and amount of TiN. Samples were sintered using three different densification methods:

(a) hot pressing (HP) under vacuum at $T=$ 1800°C and $P=30$ MPa;
(b) pressureless sintering (PS) in N_2 atmosphere at temperatures of 1850°C for 60 min, embedding the samples in a protective bed;
(c) gas-pressure sintering (GPS) at $T=1800$°C (cycle A) and $T=1850$°C (cycle B) both for 60 min; in these cycles the N_2 pressure was held at 0·3 MPa during the ramp and for the first 30 min of the soaking time and then raised up to 5 MPa for the rest of the cycle.

As a reference, a monolithic Si_3N_4 sample was produced by hot pressing at 1750°C for 30 min.

On the sintered bodies, densities were measured by the Archimedes technique. A theoretical value of 3·28 g/cm^3 was taken for the base-line matrix; for the composites, the values were calculated with the rule of mixtures assuming that no reaction takes place between the Si_3N_4 matrix and the second phase.

Microstructural characteristics were studied through X-ray diffraction, scanning electron microscopy (SEM) and microanalysis. Electrical resistivity (ρ) was measured by a four-probe method. The current intensity, supplied by a Keithley current source Mod. 220, was held under 10 mA to avoid Joule effects. The potential was measured with a Keithley Nanovoltmeter Mod. 181. The Young's modulus (E) was measured on samples 0·8 mm × 8·0 mm × 28 mm by the frequency resonance method.[15] The flexural strength (σ), or modulus of rupture (MOR), was measured on samples 3 mm × 3 mm × 30 mm in a four-point bending fixture, 26 mm as outer span and 13 mm as inner span, with a crosshead speed of 0·5 mm/min. The bars were machined lengthwise with a resin-bonded diamond wheel of 100-grit size. The last 0·1 mm of thickness was removed at 4 μm/pass. Chamfering of the edges was done in the same way. The fracture toughness (K_{Ic}) was evaluated by the direct crack measurement (DCM) method with a load of 98 N in a hardness tester Zwick 3112 using the formula proposed by Anstis *et al.*[16] On the same apparatus the Vickers microhardness (H_v 0·5) has been measured on polished surfaces with a load of 4·81 N.

The thermal expansion coefficient (α) was measured using a Netszch dilatometer in a temperature range 20–1000°C with a heating rate of 5°C/min. Oxidation resistance (W/S) was evaluated on square samples (10 mm × 10 mm × 10 mm), polished on one surface, at 500–1400°C in air for 30 h. The weight gain was continuously recorded by a TG–DTA apparatus (PL Thermal Sciences, Epsom, UK) and the oxidized surface was characterized by XRD and SEM.

2.2 Optimization of TiN grain size distribution

In a first set of experiments, TiN powders were used as received from the producer; it was then observed that large TiN aggregates in the range 50–300 μm

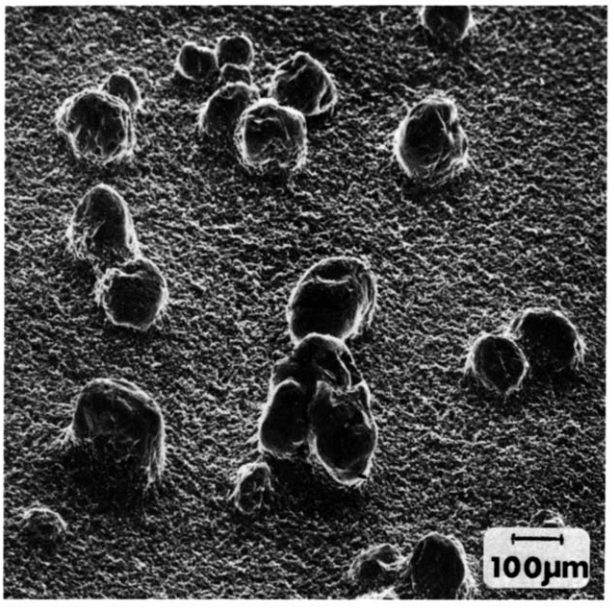

(a)

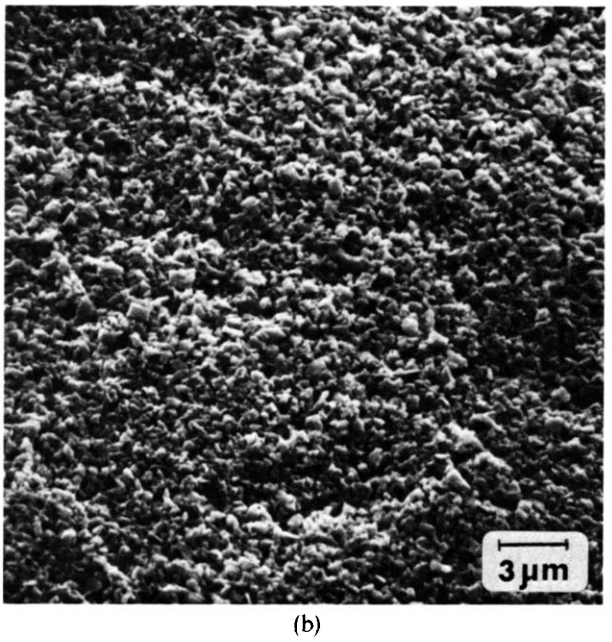

(b)

Fig. 1. Morphology of the TiN powder (a) before and (b) after the settling treatment.

(Fig. 1(a)) were the failure origins in most of the flexural strength tests. Therefore a control of the grain size has been done by sedimentation.[17] Particles with grain sizes lower than 5 μm were obtained by a series of settlings of powder suspensions at low concentration (10 wt%) using as dispersing media a mixture of ethanol/ethylene glycol in an ultrasonic bath.

The morphology and grain size of the TiN powder after this treatment are shown in Fig. 1(b).

3 Results and Discussion

The experimental results are collected in Table 1.

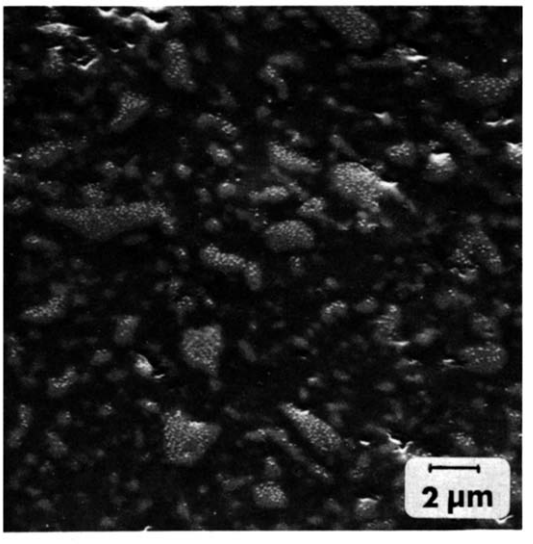

(a)

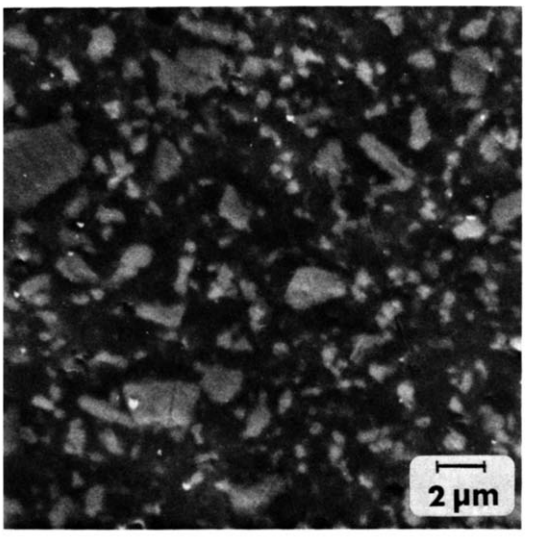

(b)

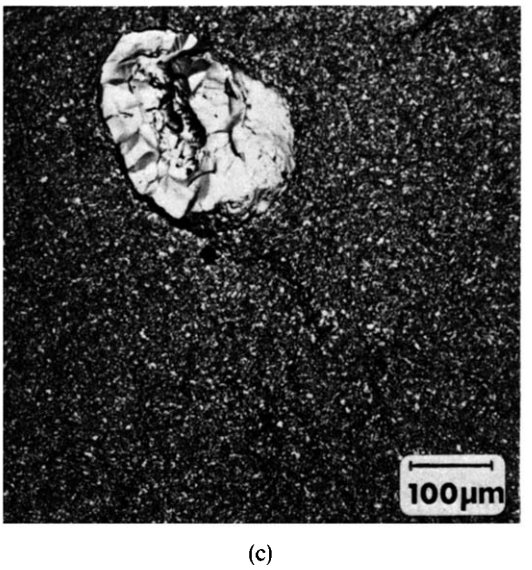

(c)

Fig. 2. Morphology of polished surfaces of a 30% TiN composite with (a) coarse TiN powder and (b) fine TiN powder. In (c) a large TiN agglomerate in a composite with coarse TiN powder is shown.

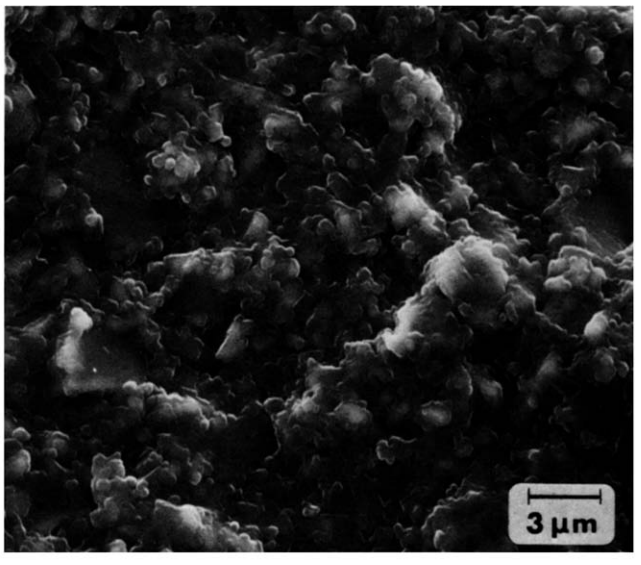

(a)

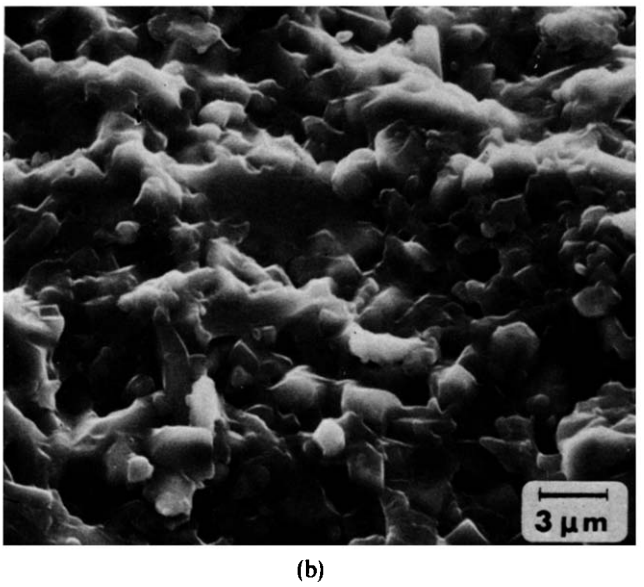

(b)

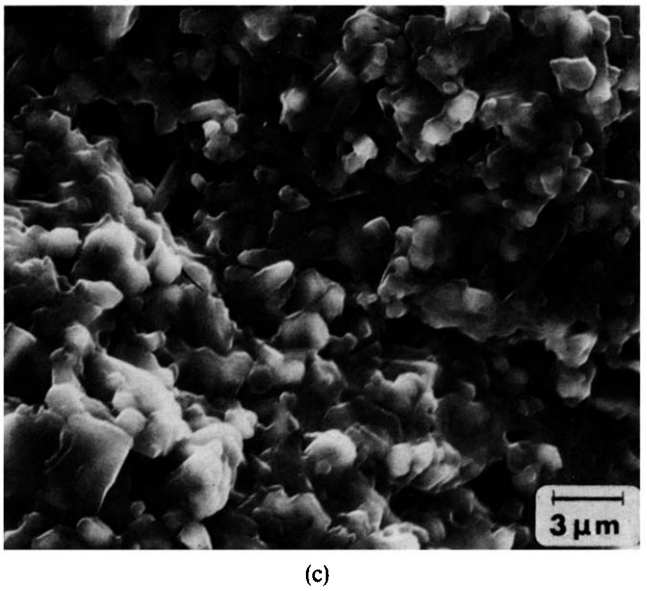

(c)

Fig. 3. Fracture surfaces showing the different microstructures in a 30% TiN composite with fine TiN powder sintered by (a) hot pressing, (b) gas-pressure sintering and (c) pressureless sintering.

3.1 Microstructure

Grain size and distribution of TiN particles in the composites produced with coarse and fine powder are shown in Fig. 2(a) and (b) (polished surfaces) respectively. In the first case, TiN particle sizes range from $\approx 0{\cdot}2$ to $\approx 7\,\mu m$ but also some large aggregates are present (Fig. 2(c)). In the second case, TiN grain sizes range from $\approx 0{\cdot}2$ to $\approx 3\,\mu m$ and no large TiN particles were found.

The influence of sintering methods and parameters on the microstructure is shown in Fig. 3(a)–(c). By hot pressing, a fine and homogeneous Si_3N_4-grain microstructure is obtained. By sintering with or without gas pressure, the higher temperatures and the longer soaking times, which are necessary to obtain high densities, promote pronounced grain growth and a prismatic morphology in the β-Si_3N_4 phase. HP and GPS composites are fully dense; the PS samples in contrast contain some porosity (see Table 1). The analysis of the matrix crystalline phase shows complete $\alpha \rightarrow \beta$-Si_3N_4 conversion and, only in HP samples, the presence of a low amount of Y_2TiO_5.

3.2 Electrical resistivity

The electrical resistivity of the composites (Table 1 and Fig. 4) decreases with increasing amount of dispersoids and reaches a minimum ($3{\cdot}5 \times 10^{-4}$ Ωcm) in the 40% TiN composite produced using fine TiN powder and gas-pressure sintering as densification method.

The electrical resistivity is governed by the formation of chains of electroconductive particles and is therefore linked to the grain size and distribution of the TiN. The effect is more evident at

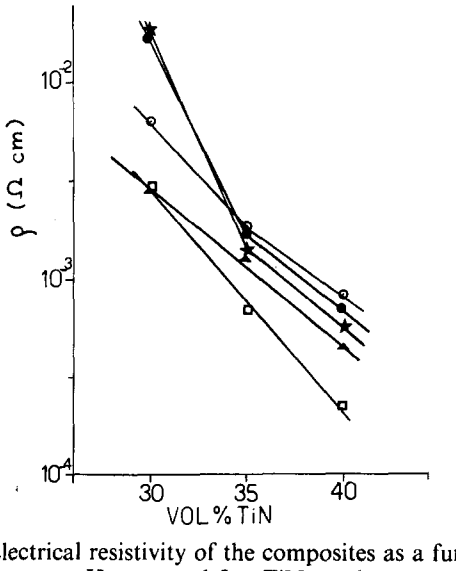

Fig. 4. Electrical resistivity of the composites as a function of TiN content. ⊙, Hot-pressed fine TiN; ●, hot-pressed coarse TiN; ★, pressureless-sintered coarse TiN; ▲, pressureless-sintered fine TiN; □, gas-pressure sintered fine TiN.

Table 1. Properties of the tested materials

Sample[a]	*Density*		ρ[b]	$H_v0{\cdot}5$[c]	E	K_{Ic}[c]	a	W/S[d]	σ[c]
	(g/cm^3)	(%)	($\Omega\,cm$)	(*GPa*)	(*GPa*)	($MPam^{1/2}$)	($\times 10^{-6}\,°C^{-1}$)	(mg/cm^2)	(*MPa*)
Hot pressing									
Si_3N_4	3·28	100	$3{\cdot}6\times10^{13}$	$20{\cdot}7\pm0{\cdot}9$	305	$4{\cdot}8\pm0{\cdot}5$	3·25	0	895 ± 35
20TiNc	3·68	99·4	$5{\cdot}0\times10^{11}$	$17{\cdot}8\pm1{\cdot}5$	318	$6{\cdot}1\pm0{\cdot}4$	4·42	0·44	545 ± 172
30TiNc	3·90	99·6	$9{\cdot}4\times10^{-2}$	$19{\cdot}2\pm0{\cdot}4$	343	$9{\cdot}0\pm1{\cdot}0$	4·68	1·17	613 ± 134
35TiNc	4·00	99·5	$2{\cdot}3\times10^{-3}$	$18{\cdot}4\pm0{\cdot}1$	354	$9{\cdot}6\pm1{\cdot}1$	4·83	—	585 ± 77
40TiNc	4·10	99·4	$8{\cdot}4\times10^{-4}$	$15{\cdot}2\pm0{\cdot}3$	358	$6{\cdot}7\pm0{\cdot}8$	5·80	1·59	529 ± 61
30TiNf	3·90	99·6	$7{\cdot}8\times10^{-3}$	$16{\cdot}3\pm0{\cdot}8$	341	$7{\cdot}5\pm0{\cdot}8$	5·05	—	889 ± 53
35TiNf	4·00	99·5	$2{\cdot}6\times10^{-3}$	$16{\cdot}3\pm0{\cdot}3$	354	$8{\cdot}0\pm0{\cdot}6$	—	—	925 ± 83
40TiNf	4·12	99·7	$9{\cdot}2\times10^{-4}$	$15{\cdot}0\pm0{\cdot}5$	360	$6{\cdot}3\pm0{\cdot}4$	—	—	$1\,043\pm21$
Gas-pressure sintering									
30TiNf[e]	3·88	99·0	$8{\cdot}7\times10^{-3}$	$14{\cdot}2\pm0{\cdot}7$	342	$6{\cdot}7\pm0{\cdot}5$	—	—	557 ± 60
30TiNf	3·94	100	$4{\cdot}7\times10^{-3}$	$15{\cdot}1\pm0{\cdot}3$	342	$7{\cdot}3\pm0{\cdot}1$	—	—	522 ± 77
35TiNf	4·01	100	$8{\cdot}5\times10^{-4}$	$14{\cdot}1\pm0{\cdot}6$	349	$8{\cdot}0\pm0{\cdot}2$	—	—	565 ± 39
40TiNf	4·15	100	$3{\cdot}5\times10^{-4}$	$14{\cdot}7\pm0{\cdot}5$	356	$7{\cdot}6\pm0{\cdot}6$	—	—	529 ± 45
Pressureless sintering									
30TiNc	3·82	97·6	$4{\cdot}7\times10^{-2}$	$11{\cdot}1\pm0{\cdot}6$	—	—	—	—	432 ± 50
35TiNc	3·78	94·0	$1{\cdot}5\times10^{-3}$	$11{\cdot}3\pm0{\cdot}6$	—	—	—	—	439 ± 73
40TiNc	3·89	94·2	$7{\cdot}6\times10^{-4}$	$9{\cdot}7\pm0{\cdot}5$	—	—	—	—	451 ± 32
30TiNf	3·64	94·1	$4{\cdot}1\times10^{-3}$	$11{\cdot}9\pm0{\cdot}4$	279	$6{\cdot}3\pm0{\cdot}3$	5·13	—	645 ± 46
35TiNf	3·86	96·0	$1{\cdot}6\times10^{-3}$	$11{\cdot}7\pm0{\cdot}3$	—	—	5·21	—	664 ± 25
40TiNf	3·94	95·0	$6{\cdot}5\times10^{-4}$	$11{\cdot}5\pm0{\cdot}5$	298	$6{\cdot}7\pm0{\cdot}8$	5·50	—	680 ± 30

[a] TiNc = coarse TiN powder; TiNf = fine TiN powder; the number refers to the second-phase volume content.
[b] See text for the explanation of the symbols.
[c] Mean ± standard deviation.
[d] Weight gain after 20 hours at 1000°C.
[e] Cycle A.

low dispersoid contents (30 vol.%) where fine particles promote a more uniform distribution and consequently a better conductivity. In contrast, the presence of coarse particles can result in some breaks in the TiN particle chains, with direct influence on the resistivity. A linear relationship exists between resistivity and the amount of TiN only when TiN fine particles are used. Therefore it can be stressed that the second-phase grain size and dispersion influence the conductivity mechanism in the composites, in agreement with the results of previous studies,[11] where the spatial fluctuations of composition were found to be the dominant factor for deviations of resistivity from a certain value which depends on the average volume fraction of the electrically conductive phase.

A relationship is also shown between sintering atmosphere and conductivity: hot pressing is performed under vacuum, leading to the formation of some Y_2TiO_5, causing a difference in conductivity between the HP composites and the others. Also an influence of the nitrogen pressure can be detected as the GPS composites exhibit the lowest values of resistivity.

3.3 Mechanical characterization

3.3.1 Young's modulus

Regardless of the sintering route used, the modulus values of the composites, either with coarse or fine TiN powder, increase with increase in TiN content, this phase being stiffer than the matrix (Table 2). In the case of PS composites the values of Young's modulus are lower than expected due to some residual porosity.

The upper (Voight) and lower (Reuss) bounds[18] calculated for the composites together with experimental results for the HP materials with coarse TiN powder are reported in Table 2. The TiN Young's modulus was taken as 469 GPa.[19] The experimental values are close to the lower bound as reported in the literature for particulate composites.[20] The value of Young's modulus for the 20% TiN composite is below the lower limit. Since this material is

Table 2. Experimental values of Young's modulus compared with the upper and lower bounds

Composite[a] (*Vol% TiN*)	E_{upper}[b] (*GPa*)	E_{lower}[c] (*GPa*)	$E_{experimental}$[d] (*GPa*)
20	338	328	318
30	354	341	343
35	362	348	354
40	371	355	358

[a] Hot-pressed samples, coarse TiN powder.
[b] $E_{upper} = E_1V_1 + E_2V_2$.
[c] $1/E_{lower} = V_1/E_1 + V_2/E_2$.
[d] Calculated by resonant frequency method.

completely dense (see Table 1), it is possible that this composite was spontaneously microcracked after the sintering cycle, due to the difference in thermal expansion between Si_3N_4 and TiN[21] ($3{\cdot}25 \times 10^{-6}\,°C^{-1}$ and $8{\cdot}0 \times 10^{-6}\,°C^{-1}$ respectively). For the system TiN–Si_3N_4, in fact, the critical dimension for spontaneous microcracking[22] is calculated to be 17 μm, that is, much lower than the size of the large agglomerates shown in Fig. 1(a). For higher TiN content this effect is not observed, but in this case part of the TiN phase is continuously connected through the matrix as the electrical resistivity clearly indicates. In this situation, the number of single particles embedded in the matrix, and responsible for the spontaneous microcracking, is greatly reduced and the modulus values are in good agreement with the theory.

3.3.2 Microhardness

In the composites, the microhardness generally decreases with increase in TiN content, this phase being softer than the matrix.[21] The HP composites with coarse TiN powder are found to be harder than the corresponding materials with fine TiN powder (Fig. 5). In the composites with coarse second phase, part of the TiN content is concentrated in large agglomerates. These agglomerates are avoided during hardness tests so that the indentations are made in zones of material with TiN content lower than the nominal one, thus giving higher results.

The hardness of the GPS composites as a function of TiN shows the same behaviour as in the HP materials: the introduction of the second phase makes the composite softer. Generally, the hardness values of the GPS materials are lower than the corresponding HP materials, since the microstructure is finer in the latter and the hardness of Si_3N_4-based materials is known to have an inverse dependence on the grain size.[23,24] The hardness value of the composite sintered with cycle A is slightly lower than the corresponding composite sintered with cycle B, probably due to the small amount of the residual porosity (see Table 1).

Being the most porous, the PS composites give the lowest values of hardness among all the materials. Here the hardness is the combined result of amount of the TiN phase and the residual porosity. In this case a unique trend of the hardness as a function of TiN content is not clear.

3.3.3 Fracture toughness

The fracture toughness of the composites increases with increasing TiN content to a maximum at 35% and then decreases. This behaviour is independent of the sintering route. The coarse HP composites are the toughest (Fig. 6 and Table 1), with all the other composites having similar toughness values. Different toughening mechanisms have been proposed for particulate composites: crack pinning,[25] crack deflections,[26] microcracking,[27] crack bridging[28] and residual stresses.[29] A number of these mechanisms can be active at the same time, making it difficult to indicate a prevailing phenomenon. Crack deflection is definitely evident, as can be seen on the fracture surfaces (Fig. 7(a) and (b)), but the fact that coarse particles are more effective in toughening indicates that mechanisms such as stress-induced microcracking and crack pinning are more likely. Alternative causes for the lowering of the fracture toughness at 40% TiN can be proposed. If crack pinning is the main mechanism, it is possible that the toughening increment is not operating fully, due to the shorter interparticle distance, i.e. the crack crosses another particle before bowing completely.[25] Alternatively, since the overall fracture toughness of a composite is determined by the toughening effect and the effective energy consumed for crack propagation,[30] it can be that for the 40% TiN composite the toughening mechanism is counterbalanced by the lower TiN fracture energy,[21]

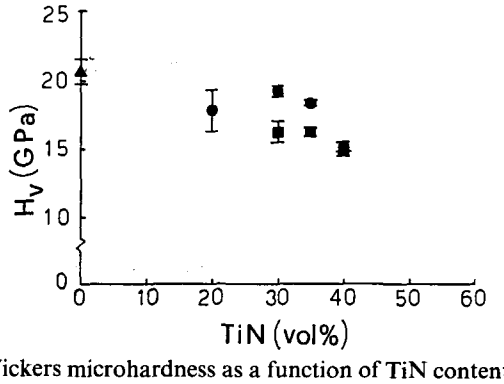

Fig. 5. Vickers microhardness as a function of TiN content for the hot-pressed composites. ▲, Hot-pressed Si_3N_4; ●, coarse TiN; ■, fine TiN.

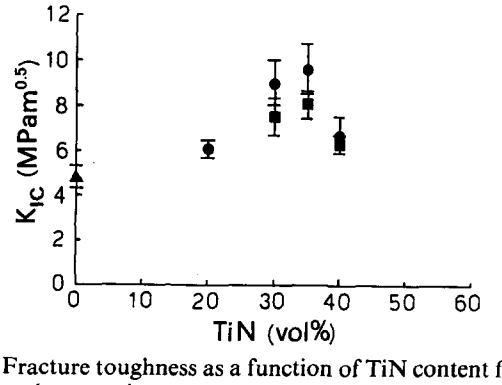

Fig. 6. Fracture toughness as a function of TiN content for the hot-pressed composites. ▲, Hot-pressed Si_3N_4; ●, coarse TiN; ■, fine TiN.

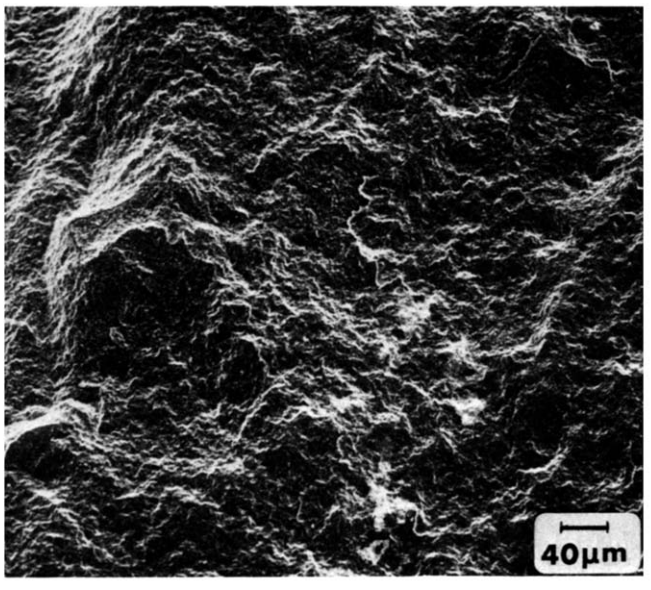

(a)

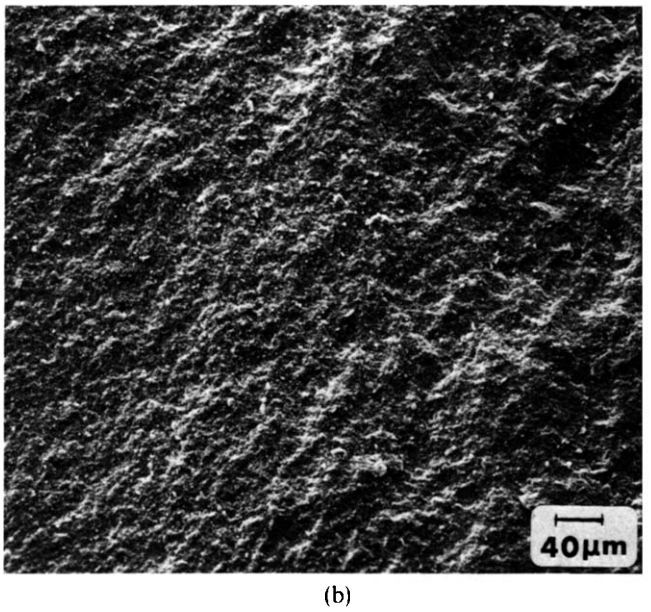

(b)

Fig. 7. Fracture surfaces of (a) a hot-pressed Si_3N_4 matrix and (b) a 30% TiN composite with coarse TiN powder. Note the evident increase in surface roughness in the composite with respect to the matrix.

i.e. the crack propagates in the more brittle material. If stress-induced microcracking is the main reason for the toughening of the composite, then microcracks coalescence ahead of the main crack can reduce the toughness, as already observed in Al_2O_3–ZrO_3 systems,[31] Al_2O_3–glass systems[32] and SiC–Al_2O_3 systems.[33]

3.3.4 Flexural strength

3.3.4.1 Room temperature. The room temperature flexural strength of the HP composites is greatly influenced by the type of TiN powder used (Fig. 8). If the as-received TiN powder is used, the larger TiN agglomerates act as fracture origins (Fig. 9) and the

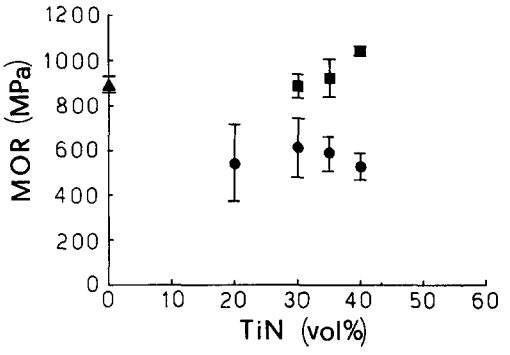

Fig. 8. Room-temperature flexural strength as a function of TiN content for the hot-pressed composites. ▲, Hot-pressed Si_3N_4; ●, coarse TiN; ■, fine TiN.

MOR of these composites is lower than that of the matrix in spite of the fracture toughness increment. When the fine TiN powder is used, the MOR of the composites is nearly the same as the matrix up to 35% TiN and then slightly improved for a TiN content of 40%. The high improvement in fracture toughness obtained in these composites, where large agglomerates are not present, did not result in a comparable strength improvement. According to the Griffith equation, higher fracture toughness should correspond to higher strength at equal defect size. The MOR values of these composites as a function of the TiN content indicate that the critical flaw size is in someways related to the second-phase content. Increasing the second-phase content can reduce the critical flaw size when the interparticle spacing is less than the critical flaw size of the matrix,[34] but if the stress-induced microcracking is the active toughening mechanism in these composites, during the loading of the sample the initial flaw of the material can subcritically grow by linking

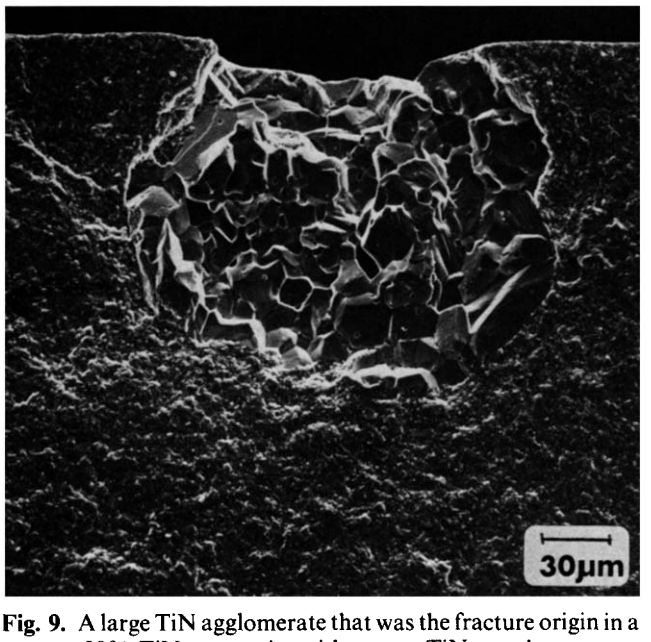

Fig. 9. A large TiN agglomerate that was the fracture origin in a 30% TiN composite with coarse TiN powder.

with the microcracks formed ahead of its front. In the present case, therefore, the experimental strength of a composite is determined by its fracture toughness, its initial flaw size and the subcritical crack growth that can occur during the loading of the sample.

Regardless of the sintering cycle used, the GPS samples have MOR values lower than the corresponding HP samples, due to their coarser microstructure. The flexural strength in these composites is independent of TiN content in the range investigated. Again, since their toughness changes, the defect populations must change with the TiN content as indicated above.

In the PS composites, the introduction of the as-received TiN powder weakens the composites with respect to those in which a finer powder is used, as already seen. Quite unexpectedly, the PS composites made with fine TiN powder are stronger than the corresponding GPS materials of higher density (see Table 1). It is likely that in these composites the stress-induced microcracking is not operating fully, since this Young's modulus of the matrix is reduced by the porosity and that influences the residual stress responsible for microcracking.[29] In this way the critical flaw should have less possibility to link with stress-induced microdefects and its initial size is relatively unchanged.

3.3.4.2 High temperature. Only the HP composites with fine TiN powder were tested at high temperature. The results of this investigation are reported in Table 3. At 800°C the decrement in respect to room temperature is evident in all samples. At 1000°C the flexural strength of the 30% TiN composite is still decreasing, but for the 35 and 40% TiN composites there is a slight improvement even if the latter value is associated with a very large scatter in experimental results. At 1000°C the MOR of these two composites is almost the same as the matrix (Table 3).

The MOR difference between room temperature and high temperature may arise from the relief of residual compressive stress introduced by the machining.[35] The temperature can, however, affect the MOR in other ways. For example, the defect population could be changed by temperature, as reported in the literature.[36] In the present case, moreover, the second phase is very reactive to oxidation and the transformation $TiN \rightarrow TiO_2$ is known to be volume-dilatant[37] with obvious consequences on surface integrity. The presence of the second phase seems to influence the spread of strength data; the standard deviations of the composites are, in general, higher than that found for the matrix (Table 3).

TABLE 3. Four-point flexural strength of the matrix and the composites as a function of the temperature[a]

Sample	*Room temperature*	*800°C*	*1000°C*
Si_3N_4	895 ± 35	—	603 ± 39
Si_3N_4 + 30% TiN	889 ± 53	528 ± 50	495 ± 110
Si_3N_4 + 35% TiN	925 ± 83	506 ± 77	611 ± 28
Si_3N_4 + 40% TiN	1043 ± 21	558 ± 21	627 ± 111

[a]All measurements are in MPa: mean value ± standard deviation.

3.4 Thermal expansion

As expected, owing to the higher thermal expansion coefficient of TiN, the thermal expansion coefficients of the composites are higher than that of the base-line material and increase almost linearly with the second-phase content (Table 1). For the compositions in the range investigated (0–40 vol.%), the experimental values of the thermal expansion coefficient are in good agreement with those calculated with the rule of mixtures, according to

$$\alpha_c = \alpha_1 V_1 + \alpha_2 V_2 \quad (1)$$

where α_c is the thermal expansion coefficient of the composite, α_1 and α_2 those of the base-line Si_3N_4 and TiN and V_1 and V_2 are the respective volume fractions.

3.5 Oxidation resistance

The thermal stability of the composites is directly related to the amount of TiN which is an easy-to-oxidize phase. Figure 10 shows the weight gain for oxidation measured during thermal treatment at 1000°C; at this temperature no weight gain is recorded for the base-line Si_3N_4 matrix. Figure 11 shows the parabolic weight gain versus time for a

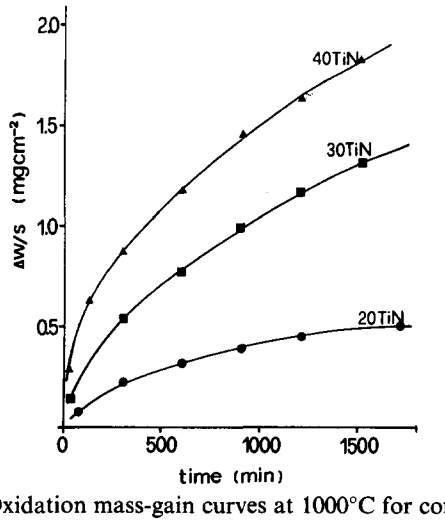

Fig. 10. Oxidation mass-gain curves at 1000°C for composites with various TiN contents. ●, 20%; ■, 30%; ▲, 40%.

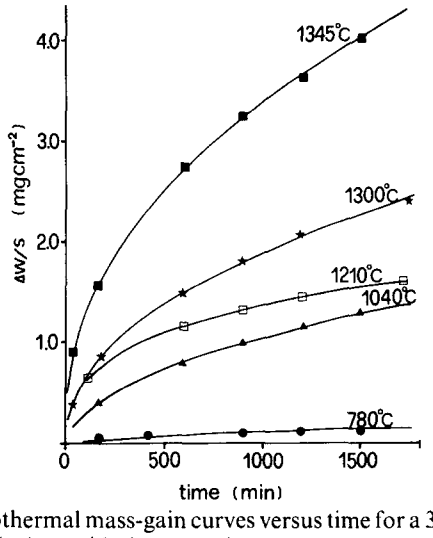

Fig. 11. Isothermal mass-gain curves versus time for a 30% TiN composite during oxidation at various temperatures. ●, 780°C; ▲, 1040°C; □, 1210°C; ★, 1300°C; ■, 1345°C.

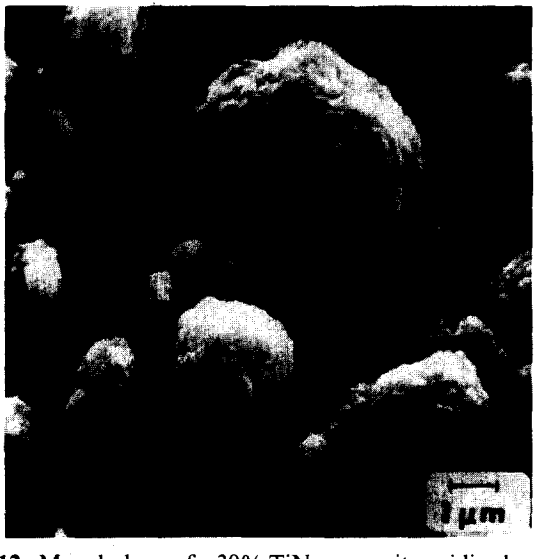

Fig. 12. Morphology of a 30% TiN composite oxidized surface at 800°C. At this temperature the oxidation takes place only in the TiN phase.

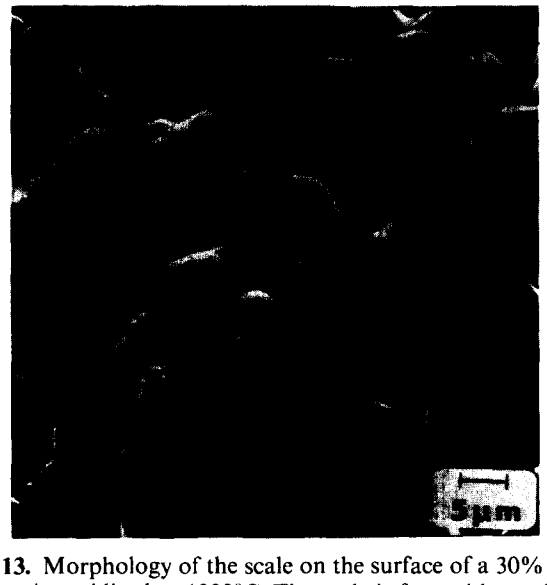

Fig. 13. Morphology of the scale on the surface of a 30% TiN composite oxidized at 1200°C. The scale is formed by a glassy phase in which TiO_2 crystals are embedded.

30% TiN composite oxidized at various temperatures. A detailed study of the phenomenon[38] has indicated that up to ≈1000°C only the reaction $TiN \rightarrow TiO_2$ takes place and that corrosion is limited to the TiN phase (Fig. 12). At $T \geq 1000$°C the Si_3N_4 matrix oxidizes, assisted by diffusion of oxygen through the TiO_2-rich surface layer. Figure 13 shows the morphology and the composition of the oxidized layer in a 30% TiN composite oxidized at 1200°C for 30 h: the oxide scale is mainly formed by a glassy silicate phase where TiO_2 crystals are present. In any case the presence of TiN is deleterious for the thermal stability at low (500–1000°C) and high (≈1000–1350°C) temperatures.

3.6 Electrical discharge machining

EDM tests were carried out on 30% and 40% TiN composites through wire EDM and die-sink EDM. Wire EDM tests were performed using a brass wire as the electrode and water as dielectric. In this case, cutting speeds of 1·5 mm/min were measured on flat cylindrical samples 1 cm high.

The roughness of the as-cut surfaces is about 4·2 and 1·7 μm/mm for 30% and 40% TiN samples respectively; a finishing run at lower frequence reduces the roughness to ≈3·5 and 0·9 μm/mm respectively. The microstructure of the EDM-treated surface of the composites shows the formation of a surface layer 10–20 μm in thickness (Fig. 14). X-Ray diffraction analysis shows the presence of TiN and only traces of Si_3N_4. In Fig. 15(a) and (b) the surface morphologies of a 40% TiN composite are compared, after wire and die-sink EDM respectively. Discharges create craters and the

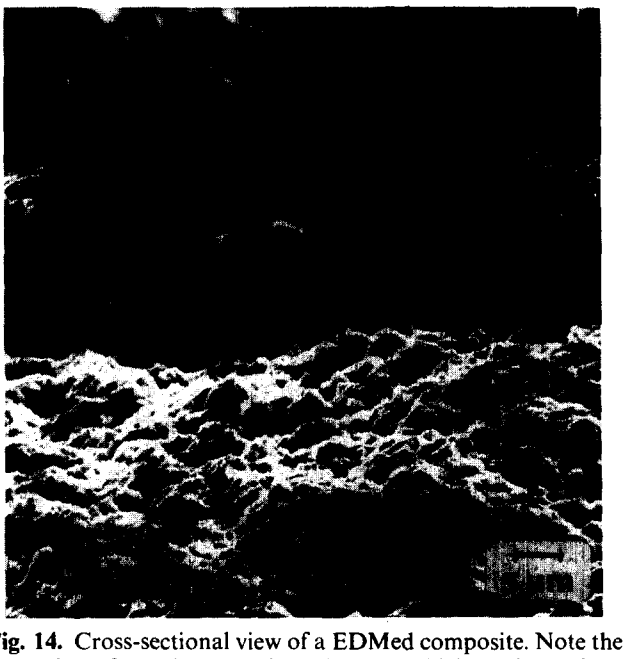

Fig. 14. Cross-sectional view of a EDMed composite. Note the formation of a scale approximately 10 μm thick on the surface.

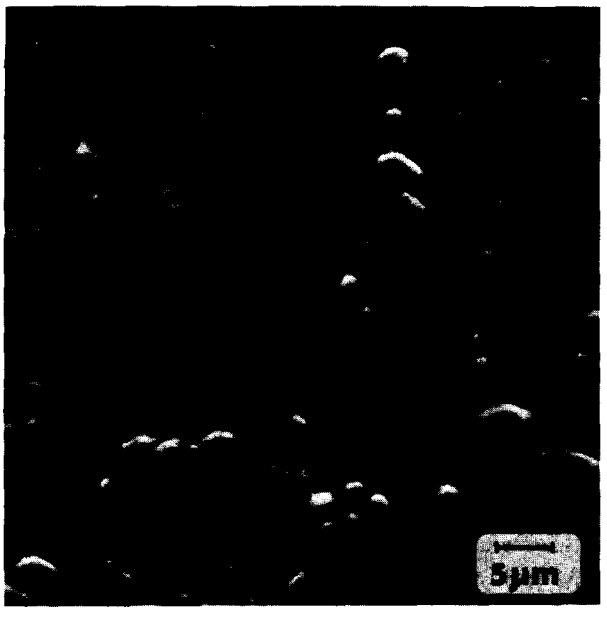

(a)

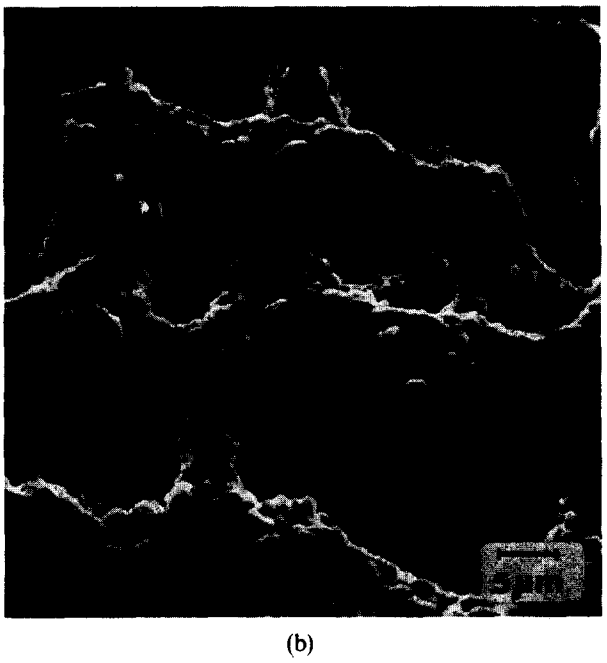

(b)

Fig. 15. Morphology of the surface in a 30% TiN composite EDMed by (a) wire technique and (b) die-sink technique.

overall surface has a superposition of craters with varying diameters and positions. This is the result of discrete, random pulses with varying intensity and spatial distribution, i.e. they derive from the material removing mechanisms which are linked to the interaction between the material and the methods and parameters adopted during EDM.

During the EDM of these materials, two main mechanisms should be involved: melting and evaporation.[39,40] Therefore the surfaces are covered by layers with resolidified-melt-formation droplets. The quantity of material that solidifies and adheres to the surface is a function of the composition and microstructure of the ceramic and of the EDM processing conditions. In the present case the resolidified droplets are almost entirely TiN as Si_3N_4 should be removed by evaporation.

4 Conclusions

The main target was to produce electroconductive composites without detrimental effects on the mechanical properties of the matrix. Using an as-received and a refined TiN powder, Si_3N_4–TiN composites in the range 0–40 vol.% TiN were produced by hot pressing, gas-pressure sintering and pressureless sintering.

Fully dense materials (>99%) were obtained by hot pressing and gas-pressure sintering in all the composition ranges investigated. For a TiN content >30 vol.%, the resistivity of the composites was some $10^{-4}\,\Omega$cm, against the $10^{11}\,\Omega$cm of the matrix, confirming the suitability of these materials for EDM.

When TiN particles are added to the Si_3N_4 matrix, the Young's modulus and the thermal expansion coefficient increase regardless of the TiN particle size and sintering route. In contrast, other mechanical properties like hardness, fracture toughness and flexural strength are strongly influenced by these two factors. Hardness and fracture toughness are higher in the composites with coarse TiN particles, but the flexural strength of these materials is lower than that in composites with fine TiN particles. Hot pressing was found in the present work to be the best sintering route in order to obtain high-performance composites.

The flexural strength of the HP composites decreased with increasing temperature. At 1000°C the flexural strength of the composites and of the base-line Si_3N_4 were at the same level; the larger scatter in experimental results for the composites indicated an influence of the second phase at high temperature. Titanium nitride is an easy-to-oxidize phase and its presence is deleterious for chemical stability: composites were rapidly oxidized already at 800°C where the matrix is virtually inert.

References

1. Shalek, P. D., Petrovic, J. J., Hurley, G. F. & Gac, F. D., Hot-pressed SiC whiskers/Si_3N_4 matrix composites. *Am. Ceram. Soc. Bull.*, **65** (1986) 351–6.
2. Greil, P., Petzow, G. & Tanaka, H., Sintering and HIPping of silicon-nitride–silicon-carbide composite materials. *Ceram. Int.*, **13** (1987) 19–25.

3. Buljan, S. T., Baldoni, J. G. & Huckabee, M. L., Si_3N_4–SiC composites. *Am. Ceram. Soc. Bull.*, **66** (1987) 347–52.
4. Bellosi, A. & de Portu, G., Hot-pressed Si_3N_4–SiC whiskers composites. *Mat. Sci. Eng.*, **A109** (1989) 357–62.
5. Buljan, S. T. & Zilberstein, G., Microstructure development in Si_3N_4-based composites. In *Mat. Res. Soc. Symp. Proc. Vol. 78. Advances in structural ceramics*, ed. P. F. Becher, M. V. Swain and S. Sōmiya, Material Research Society, Pittsburgh, Pennsylvania, 1987, pp. 273–81.
6. Jimbou, R., Takahashi, K., Matsushita, Y. & Kosugi, T., SiC–ZrB_2 electroconductive ceramic composites. *Adv. Ceram. Mat.*, **1** (1986) 341–5.
7. McMurtry, C. H., Boecker, W. D. G., Seshadri, S. G., Zanghi, J. S. & Garnier, J. E., Microstructure and material properties of SiC–TiB_2 particulate composites. *Am. Ceram. Soc. Bull.*, **66** (1987) 325–9.
8. Martin, C., Mathieu, P. & Cales, B., Electrical discharge machinable ceramic composite. *Mat. Sci. Eng.*, **A109** (1989) 351–6.
9. Matsushita, Y., Nakamura, K. & Kosugi, T., US Patent No. 4 528 121, 2 July 1985.
10. Endo, H., Tanemoto, K. & Kubo, H., European Patent No. 0243963-A2, 30 April 1987.
11. Takahashi, K. & Jimbou, R., Effect of uniformity on the electrical resistivity of SiC–ZrB_2 ceramic composites. *J. Am. Ceram. Soc.*, **70** (1987) C369–C373.
12. Bellosi, A., Fiegna, A. & Babini, G. N., Electroconductive Si_3N_4-based composites. In *Euro-Ceramics*, Vol. 3, ed. G. deWith, R. A. Terpstra & R. Metseelar. Elsevier Applied Science Publishers, London, 1989, pp. 389–93.
13. Petrofes, N. F. & Gadalla, A. M., Electrical discharge machining of advanced ceramics. *Am. Ceram. Soc. Bull.*, **67** (1988) 1048–52.
14. Ramulu, M., EDM sinker cutting of a ceramic particulate composite, SiC–TiB_2. *Adv. Ceram. Mat.*, **3** (1988) 324–7.
15. ASTM C848-78 (Reapproved 1983).
16. Anstis, G. R., Chantikul, P., Lawn, B. R. & Marshall, D. B., A critical evaluation of indentation technique for measuring fracture toughness: I. Direct crack measurements. *J. Am. Ceram. Soc.*, **64** (1981) 533–8.
17. Roncari, E. & Fanti, F., Internal Report CNR-IRTEC No. 89-009.
18. Sendeckyj, G. P., Elastic behaviour of composites. In *Composites Materials*, Vol. 2, ed. L. J. Brontman & R. H. Crock. Academic Press, New York, 1974, pp. 45–83.
19. Desmaison-Brut, M., Glandus, J. C., Montintin, J., Valin, F. & Boncour, M., Elastic moduli–porosity relations in transition metal nitrides: TiN, ZrN, HfN and TaN. Presented at 7th CIMTEC, Montecatini, Italy, June 1990.
20. Ashby, M. F. & Jones, D. R. H., *Engineering Materials*. Pergamon Press, Oxford, 1980.
21. Ceramic Source, 90, Vol. 5, Am. Ceram. Soc. Inc., Westerville, Ohio, p. 315 (1989).
22. Magley, D. J., Winholtz, R. A. & Faber, K. T., Residual stresses in two-phase microcracking ceramic. *J. Am. Ceram. Soc.*, **73** (1990) 1641–4.
23. Babini, G. N., Bellosi, A. & Galassi, C., Characterization of hot-pressed silicon nitride-based materials by microhardness measurements. *J. Mat. Sci.*, **22** (1987) 1687–93.
24. Mukhopadhyay, A. K., Datta, S. K. & Chakraborty, D., On the microhardness of silicon nitride and sialon ceramics. *J. Eur. Ceram. Soc.*, **6** (1990) 303–11.
25. Green, D. J., Fracture toughness predictions for crack bowing in brittle particulate composites. *J. Am. Ceram. Soc.*, **66** (1983) C4–C5.
26. Faber, K. T. & Evans, A. G., Crack deflection processes—I. Theory. *Acta Met.*, **31** (1983) 565–76.
27. Evans, A. G. & Faber, K. T., Toughening of ceramics by circumferential microcracking. *J. Am. Ceram. Soc.*, **64** (1981) 394–98.
28. Budiansky, B., Amazigo, J. C. & Evans, A. G., Small-scale crack bridging and the fracture toughness of particulate-reinforced ceramics. *J. Mech. Phys. Solids*, **36** (1988) 167.
29. Taya, M., Hayashi, S., Kobayashi, A. S. & Yoon, H. S., Toughening of a particulate-reinforced ceramic-matrix composite by thermal residual stress. *J. Am. Ceram. Soc.*, **73** (1990) 1382.
30. Lange, F. F., Fracture of brittle matrix, particulate composites. In *Composite Materials*, Vol. 4. ed. L. J. Brontman & R. H. Crock, Academic Press, New York, 1974, p. 1.
31. Claussen, N., Steeb, J. & Pabst, R. F., Effect of induced microcracking on the fracture toughness of ceramics. *Am. Ceram. Soc. Bull.*, **56** (1977) 559.
32. Miyata, N., Ichikawa, S. & Jimo, H., Fracture behaviour of brittle matrix, particulate composites with thermal expansion mismatch. In *Fracture Mechanics of Ceramics*, Vol. 7, ed. R. C. Bradt, A. G. Evans, D. P. H. Hasselman & F. F. Lange. Plenum Press, New York, 1986, p. 87.
33. Niihara, K., Nakahira, A., Uchiyama, T. & Hirai, T., High-temperature mechanical properties of Al_2O_3–SiC composites. In *Fracture Mechanics of Ceramics*. Vol. 7, ed. R. C. Bradt, A. G. Evans, D. P. H. Hasselman & F. F. Lange. Plenum Press, New York, 1986, p. 103.
34. Hasselmann, D. P. H. & Fulrath, R. M., Proposed fracture theory of a dispersion-strengthened glass matrix. *J. Am. Ceram. Soc.*, **49** (1966) 68.
35. Johnson-Walls, D., Evans, A. G., Marshall, D. B. & James, M. R., Residual stresses in ceramic surfaces. *J. Am. Ceram. Soc.*, **69** (1986) 47.
36. Evans, A. G., Engineering property requirements for high performance ceramics. *Mat. Sci. Eng.*, **71** (1985) 3.
37. Mukerji, J. & Biswas,. S. K., Synthesis, properties and oxidation of alumina–titanium nitride composites. *J. Am. Ceram. Soc.*, **73** (1990) 142.
38. Bellosi, A., Tampieri, A. & Liu, Yu-Z., Oxidation behaviour of electroconductive Si_3N_4–TiN composites. *Mat. Sci. Eng.*, **A127** (1990) 115–22.
39. Tokura, H., Kodoh, I. & Yoshikawa, H., Ceramic material processing by electrical discharge in electrolyte. *J. Mat. Sci.*, **24** (1989) 981–98.
40. Ramulu, M. & Taya, M., EDM machinability of SiC_w/Al composites. *J. Mat. Sci.*, **24** (1989) 1103–8.